

Article

Effect of the Cooling Regime on the Mineralogy and Reactivity of Belite-Sulfoaluminate Clinkers

Sabina Dolenc^{1,*}, Katarina Šter¹, Maruša Borštnar¹, Klara Nagode² , Andrej Ipavec³ and Lea Žibret¹

¹ Slovenian National Building and Civil Engineering Institute, Dimičeva ulica 12, 1000 Ljubljana, Slovenia; katarina.ster@zag.si (K.Š.); marusa.borstnar@zag.si (M.B.); lea.zibret@zag.si (L.Ž.)

² Jožef Stefan Institute, Jamova 39, 1000 Ljubljana, Slovenia; klara.nagode@ijs.si

³ Salonit Anhovo Joint-Stock Co, Anhovo 1, 5210 Deskle, Slovenia; andrej.ipavec@salonit.si

* Correspondence: sabina.dolenc@zag.si

Received: 4 September 2020; Accepted: 12 October 2020; Published: 15 October 2020



Abstract: This study investigated the influence of different cooling regimes on the microstructure and consequent reactivity of belite-sulfoaluminate clinkers. The cement clinkers were synthesized by incorporating secondary raw materials, such as titanogypsum and bottom ash, to the natural raw materials. Clinker phases were determined by Rietveld quantitative phase analysis, while the distribution morphology and the incorporation of substitute ions in the phases were characterized by scanning electron microscopy using energy-dispersive X-ray spectroscopy (SEM/EDS). Clinker reactivity was studied using isothermal calorimetry and was additionally investigated through compressive strength, which was determined for the cement prepared from the synthesized clinkers. X-ray diffraction analysis showed that, as well as the three main phases (belite, calcium sulfoaluminate, and ferrite), the clinkers contained additional minor phases (mayenite, gehlenite, arkanite, periclase, and perovskite), the ratios of which varied according to the cooling regime utilized. Microscopic observations indicated that the cooling regime also influenced the crystal size and morphology of the main phases, which consequently affected clinker reactivity. Furthermore, a smaller amount of substitute elements was incorporated in the main phases when cooling was slowed. Results showed that, in comparison to clinkers cooled at slower rates, air quenched clinkers reacted faster and exhibited a higher compressive strength at 7 days.

Keywords: clinkers; belite; calcium sulfoaluminate; cooling; microstructure; reactivity

1. Introduction

The cooling regime is one variable that has a significant impact on the phases produced during the clinking process and, consequently, on the reactivity of the clinker phases and, ultimately, the properties of the cement produced [1,2]. While studies mainly concern the development and behavior of individual clinker phases with respect to the parameters, such as reactant concentrations, heating temperature, and time [3,4], less attention has been given to the mineralogy of the cooling process. The rate at which cement clinkers are cooled has long been known to be an important factor in the quality of ordinary Portland cement (OPC), while noticeably different mineral properties between different samples have been noted [3,5]. It has been observed that a variation in cooling rate not only influences the changes associated with the phase composition, morphology, crystal sizes, amorphous phase, or reactivity of phases but also affects their structure and, most importantly, the properties of the binders obtained from them [6,7]. Bullard [2] showed a definite trend towards simplicity of the crystal form and clinker structure as the cooling rate increased, with the overall size of all clinker phases being smaller following faster cooling. In addition to temperature and substitute ions, the polymorphisms of

clinker phases are a function of the cooling rate [8]. Furthermore, the chemical and phase compositions in the clinker interstitial phase vary significantly depending on the cooling rate [9], with fast cooling increasing the likelihood of other elements (e.g., Mg, Al, Fe, etc.) becoming trapped in the crystal structure of the clinker silicate phases. Such chemical substitutions cause the clinker phases to become more reactive during hydration, thus shortening the setting time of cements and ultimately increasing their strength. Moreover, microtextures of belite crystals have been shown to vary according to the cooling conditions, i.e., quenching temperature and cooling rate [10].

While the clinkerization of conventional OPC clinkers has been extensively investigated over the past decades, there are only a limited amount of studies discussing the clinkerization processes of belite-sulfoaluminate cement clinkers in detail [11–15]. Belite-sulfoaluminate cements are potentially an alternative cementitious binder to OPC cements, due to the lower embodied energy and CO₂ emissions required compared to OPC clinker production, resulting from a lower limestone requirement, lower grinding energy, and lower clinkering temperatures [16,17]. The main mineral analogs in belite-sulfoaluminate clinker are larnite (belite, C₂S) and sodalite-type ye'elimite (C₄A₃S̄), also called Klein's salt tetracalcium aluminate sulfate or calcium sulfoaluminate. There is a wide range of compositions possible within the frame of belite-sulfoaluminate clinkers (BCSA). Nowadays, the research stream is strongly focused on iron-rich BCSA clinkers, which are also referred to in the literature as belite-calcium sulfoaluminate-ferrite BCSAF clinkers [18] or belite-ye'elimite-ferrite clinkers (BYF) [17]. In the literature, iron-rich BCSA clinkers are described to have a targeted phase composition of 40–70 wt.% belite, calcium sulfoaluminate is usually in the range 20 to 40 wt.%, and brownmillerite-type ferrite (C₄AF) varies from 10 to 25 wt.% [13,19–22]. Since ternesite has been proved to be a reactive phase in iron-rich BCSA clinkers [13], another variety of iron-rich BCSA clinkers, so called BCT (belite-calcium sulfoaluminate-ternesite) clinkers, has been developed [23]. BCSA clinkers may also contain other minor phases, such as mayenite (C₁₂A₇), gehlenite (C₂AS), perovskite (CT), periclase (M), and excess anhydrite (CaSO₄) [11,14,24–27].

The phase composition of these clinkers has been investigated under different heating profiles, most commonly involving variations in clinkering temperature, as well as retention times [11], sometimes involving nonlinear heating. The studies are mostly focused on investigating the optimum firing temperature, at which a particular phase is formed—depending on the variable raw meal compositions. The most common cooling regimes used in these studies was air quenching [11,12] or natural cooling [24]. On the other hand, Bullerjahn et al. [13] studied different clinkering processes and demonstrated that it is possible to vary the hydration kinetics of BCSAF-based clinkers by applying specific clinkering processes and by changing the design of the raw mix accordingly. However, none of the previous studies [11–13,24] were focused on the influence of the cooling regime on the mineralogy and reactivity of BCSA clinkers. Namely, each of the abovementioned studies investigated BCSA clinkers with different phase compositions or used different raw materials for the clinker preparation. Therefore, the influence of the cooling regime on the microstructure of BCSA clinkers cannot be revealed from the existing studies.

The aim of the study was to investigate the effects of different cooling regimes on the mineralogy and microstructure of BCSA clinkers and the subsequent impact on their reactivity. BCSA clinkers of uniform phase and oxide composition were subjected to uniform heating rate and holding time. In order to reveal the influence of cooling regime on the BCSA clinker microstructure and reactivity, clinkers were subjected to three different cooling rates; fast cooling (air-quenching), slow cooling (1 °C/min), and an intermediate example with a combination of cooling with a constant cooling rate of 10 °C/min to 850 °C and air quenching.

2. Materials and Methods

2.1. Materials

Cement clinkers with a nominal phase composition of 65wt.% β - C_2S , 20wt.% C_4A_3S , and 10wt.% C_4AF were synthesized for the study (calculated to main phases $\Sigma 95\%$). The clinkers were synthesized from ratios of limestone, flysch, calcined bauxite, white titanogypsum, coal bottom ash, and mill scale. The chemical composition of the raw meal was given in Table 1, while the chemical composition of the raw materials and their proportions for the raw mix was given in a previous study [28].

Table 1. Chemical composition of the clinker raw meal (WD-XRF, Thermo Scientific ARL PERFORM'X, Thermo Fisher Scientific, Massachusetts, USA; fused beads, UniQuant program).

Chemical Composition	CaO	SiO ₂	Al ₂ O ₃	Fe ₂ O ₃	SO ₃	MgO	K ₂ O	TiO ₂	Na ₂ O	LOI	Total
wt.%	35.45	16.28	9.51	2.44	1.25	1.09	0.58	0.43	0.30	30.62	97.95

All raw materials were first ground passed through a 200 μ m sieve. The raw mixture (200 g for each cooling regime) was then homogenized and ground for 3 h in 200 ml of isopropanol using a ball mill (CAPCO Test Equipment Ball Mill Model 9VS, Capco Test Equipment, Ipswich, UK). Pressed pellets were prepared using an HPM 25/5 press at 10.6 kN. For each pellet (diameter 30 mm), 15 g of material was used.

The clinker mixtures were subjected to the following heating regime: Heating to 1300 °C at a heating rate of 10 °C/min followed by 60 min holding time at the final temperature. Three different cooling regimes followed: (1) Air quenching, (2) nonlinear cooling with a constant cooling rate of 10 °C/min to 850 °C, followed by air quenching, and (3) slow cooling at a constant cooling rate of 1 °C/min. The heating and cooling were carried out under oxidizing conditions.

After heating, all clinkers were ground to a fineness below 0.125 mm, and the cement was prepared by adding 20.3 wt.% of white titanogypsum (ground below 0.125 mm) and mixing by dry homogenization for 2 h. The amount of gypsum needed was calculated according to the method outlined by Chen and Juenger [25]. The Blaine specific surface area (SSA) and particle size distribution of the ground clinkers and prepared cement were shown in Table 2 and Figure 1.

Table 2. Specific surface area (Blaine method, ToniPERM Standard Model 6578, ToniTechnic by Zwick, Ulm, Germany) of the ground clinkers and prepared cements.

Blaine SSA	Clinkers			Cements		
	Air Quenching	Nonlinear	Slow Cooling	Air Quenching	Nonlinear	Slow Cooling
SSA cm ² /g	2740	2760	3270	2420	2580	2960

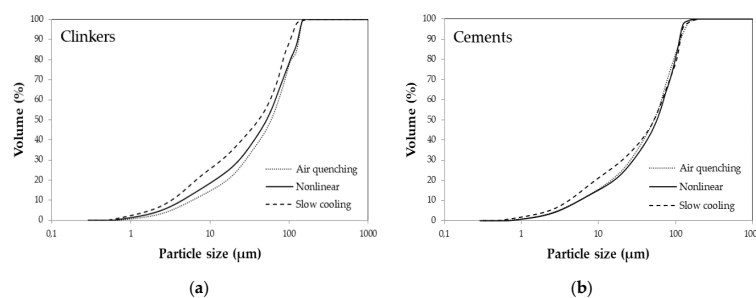


Figure 1. Particle size distribution (PSD) of the ground clinkers (a) and prepared cements (b) as determined by laser diffraction (Microtrac SYNC Model 5001, Microtrac Retsch GmbH, Haan, Germany; dry operation).

2.2. Methods

The phase composition of clinkers was determined using X-ray diffraction using a PANalytical Empyrean X-ray diffractometer (Malvern Panalytical, Malvern, UK) equipped with CuK α radiation at $\lambda = 1.54$ Å. The samples were milled to a particle size of less than 63 μm . The ground powder was manually backloaded into a circular sample holder (diameter 10 mm) to mitigate the preferred orientation effect for XRD data collection. The data were collected at 45 kV and a current of 40 mA, over the 2θ range from 4 to 70, at a scan rate of 0.026 $2\theta/\text{min}$. The obtained data were analyzed using X'Pert High Score Plus diffraction software v.4.8 from PANalytical (Malvern Panalytical, Malvern, UK), using PANICSD v.3.4 powder diffraction files (Malvern Panalytical, Malvern, UK). All Rietveld refinements were done using the PANalytical X'Pert High Score Plus diffraction software (Malvern Panalytical, Malvern, UK), using the structures for the phases from ICDD PDF4+ 2016 RDB powder diffraction files (ICDD, International Centre for Diffraction Data, Pennsylvania, USA) and publication references. The powder diffraction file (PDF) codes for the identified phases used for Rietveld refinements were: $\beta\text{-C}_2\text{S}$ (00-033-0302), $\gamma\text{-C}_2\text{S}$ (98-008-1095), $\text{C}_4\text{A}_3\text{S}$ -orthorhombic (01-083-9042), $\text{C}_4\text{A}_3\text{S}$ -cubic (01-083-7086), C_4AF (98-009-8836), CT (00-022-0153), C_{12}A_7 (98-026-1586), C_2AS (98-015-8171), K_2S (00-005-0613), and M (00-043-1022). The amorphous phase was not considered.

The polished cross-sections of the clinker samples were examined using a JEOL IT500 LV Scanning Electron Microscope (SEM) (JEOL Ltd. Tokyo, Japan) equipped with an Energy Dispersive X-ray spectrometer (EDS) (JEOL Ltd. Tokyo, Japan) with a W-filament, operated at an accelerating voltage of 20 kV in low vacuum mode and a working distance of 10 mm. In every clinker, the composition of particular main phase (belite, calcium sulfoaluminate, ferrite) was analyzed at 30 points. The size of the belite and calcium aluminate phase was determined at 144 to 139 crystals for every clinker.

Clinker reactivity was assessed by isothermal conduction calorimetry using a TAM Air calorimeter (TA Instruments, Delaware, USA). 12 g of clinker (ground below 0.125 mm) with a water/clinker ratio of 0.4 was mixed for 1 min with an Ultra Turrax tube dispenser (IKA, Delft, Netherlands), then 5.6 g of mixed paste was placed into glass vials and then immediately into the calorimeter. Heat evolution was evaluated for 4 days at 20 °C. The hydraulic reactivity of cement was assessed using the same procedure.

In order to determine the compressive strength of cement, the cement pastes with a water/cement (w/c) ratio of 0.5 were cast into prismatic molds, 10 \times 10 \times 25 mm. The samples of cement paste were demolded 24 h after casting and cured in sealed plastic bags under laboratory conditions at T (21 \pm 2) °C and 95% RH until testing. After 7 days, the compressive strength was determined on 4 specimens per mixture using a ToniNORM (ToniTechnic by Zwick, Ulm, Germany) testing machine at a loading rate of 0.05 kN/s.

3. Results and Discussion

3.1. X-Ray Powder Diffraction

The results of X-ray powder diffraction (Table 3, Figure 2) showed that the cooling regime influenced the phase composition of the clinkers, in particular the amounts of the minor phases present.

Table 3. The phase composition of the clinkers as determined using the Rietveld method (wt.%).

Phases	Air Quenching	Nonlinear	Slow Cooling
$\beta\text{-C}_2\text{S}$	67.3	65.6	65.7
$\gamma\text{-C}_2\text{S}$	1.4	3.0	5.0
$\Sigma\text{C}_2\text{S}$	68.7	68.6	70.7
o- $\text{C}_4\text{A}_3\text{S}$	11.0	9.9	11.5
c- $\text{C}_4\text{A}_3\text{S}$	7.6	7.1	5.5
$\Sigma\text{C}_4\text{A}_3\text{S}$	18.6	17.0	17.0
C_4AF	5.3	8.1	6.8

Table 3. Cont.

Phases	Air Quenching	Nonlinear	Slow Cooling
CT	1.9	1.0	0.8
C ₁₂ A ₇	2.9	1.4	0.2
C ₂ AS	0.2	1.4	2.1
K \acute{S}	1.6	1.5	1.5
M	0.8	0.9	0.9

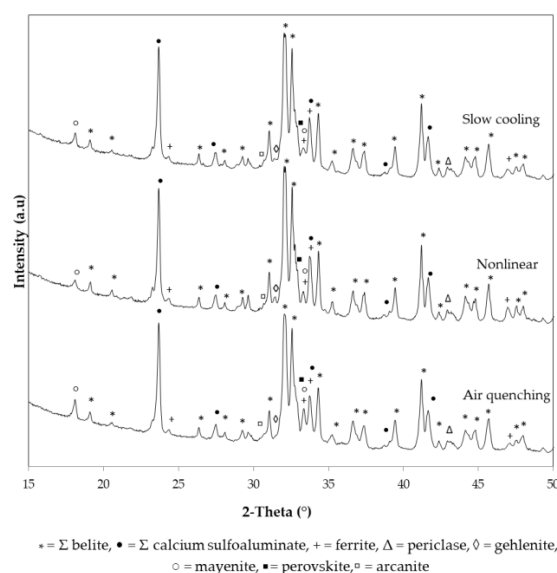


Figure 2. X-ray diffraction patterns of cement clinkers with different cooling regimes.

With regard to the main clinker phases, β -belite (β -C₂S) was the main dicalcium silicate polymorph formed with the greatest amount being observed following air quenching. The amount of γ -belite (γ -C₂S), the low-temperature polymorph of dicalcium silicate, was, however, lowest in this sample, but highest in the slowly cooled sample, as a consequence of the prolonged cooling rate [29]. This phase was formed on cooling by the polymorphic transformation, β -belite \rightarrow γ -belite, but it was hydraulically inactive and, therefore, its presence in the clinkers was undesirable [11]. Moreover, the amount of calcium sulfoaluminate or ye'elimite (C₄A₃ \acute{S}), which was present in orthorhombic and cubic form, was relatively constant in all samples. The crystal structure of ye'elimite at room temperature has been reported to be cubic, tetragonal, and orthorhombic. However, one study recently showed the reversible phase transition on heating of the orthorhombic to a higher symmetry phase, the latter likely being pseudocubic or cubic [30], while some studies have proved their orthorhombic crystal structure [31,32]. The amount of the ferrite phase (C₄AF) was slightly lower with respect to the targeted composition and rather suppressed with the fastest cooling. On the other hand, perovskite (CT) was preferred by the fastest cooling rates. Anyway, the structure of the ferrite phase Ca₂(Al_xFe_{1-x})₂O₅ derived from that of perovskite through the substitution of Al and Fe for Ti [29]. The titanium dioxide was mainly incorporated by the use of calcined bauxite, which contained 3.71 wt.% of TiO₂ [28].

Several minor phases were also observed. While mayenite was highest for the air quenched clinker, feebly hydraulic gehlenite increased with a slower cooling rate. Moreover, arcanite (K \acute{S}) and periclase (M) were identified in all samples, as a consequence of K₂O and MgO being incorporated primarily by bottom ash and flysch, respectively [28].

3.2. SEM/EDS

The influence of the different cooling regimes on the development of microstructure and phase composition was further studied using SEM/EDS. From Figures 3 and 4, variations in the particular

phase distributions were evident. Furthermore, the cooling regime also affected the pore development, i.e., the nonlinearly cooled clinker had the highest number of pores, while the smallest number of pores was observed in the air quenched clinker sample.

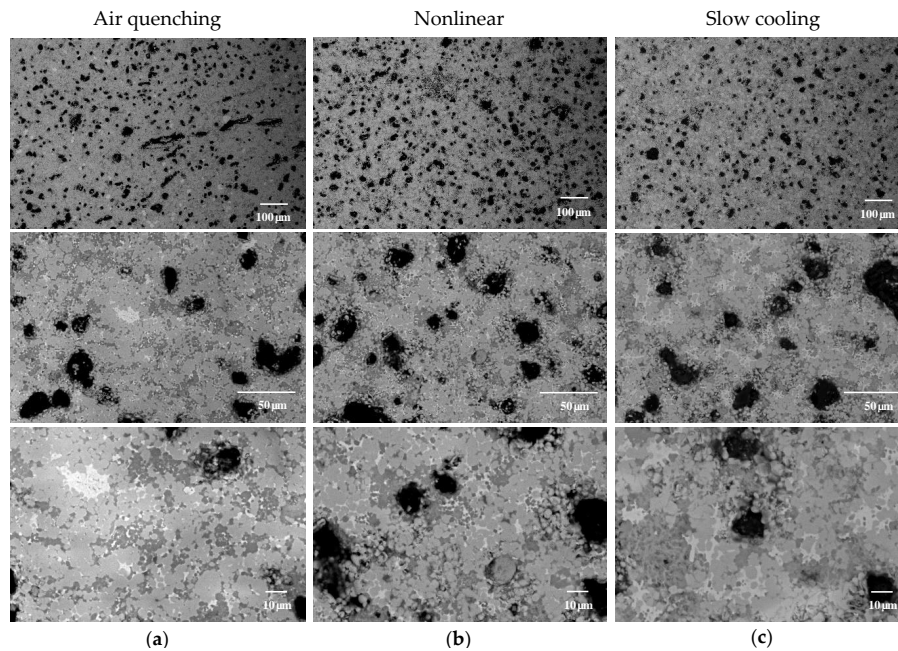


Figure 3. SEM/BSE microphotographs of cement clinkers subjected to different cooling regimes showing their microstructure at different magnifications. (a) Air quenched clinker; (b) Nonlinearly cooled clinker; (c) Slowly cooled clinker.

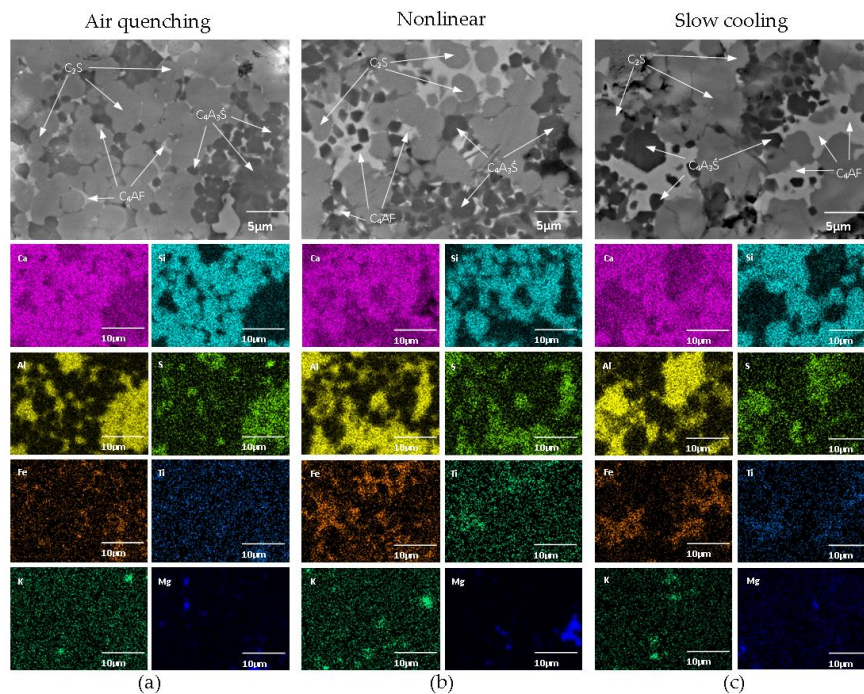


Figure 4. SEM-BSE images and the corresponding energy dispersive X-ray spectrometer (EDS) elemental mapping of the clinkers with main clinker phases marked (C_2S = belite, C_4A_3S = calcium sulfoaluminate, C_4AF = ferrite) for air quenched clinker (a), nonlinearly cooled clinker (b), and slowly cooled clinker (c).

The air quenched clinker sample showed a holocrystalline texture, meaning they were composed entirely of crystals, i.e., having no glassy part. Pores were rounded to subrounded, mostly isometric, from 3 to 40 μm in size; elongated pores were also observed, up to 200 μm in size. The dominant phase was represented by euhedral to subhedral rounded belite crystals, which were more or less uniformly-sized, from 0.6 to 5.2 μm in size. Most of the grains ranged in size from 2 to 4 μm . Belite grains were commonly clustered together (Figure 3), with the grains principally joined by crystal faces or necks, and dispersed crystals present only rarely. The calcium sulfoaluminate phase, which consisted of smaller grains compared to belite, appeared in clusters but also as an interstitial phase among belite grains. Individual crystals, however, were also found to be dispersed in the ferrite phase. In the majority, the calcium sulfoaluminate phase was not very well differentiated, having an irregular shape, but well-developed grains were observed in some places. The grains were subhedral to anhedral, euhedral from 0.3 to 4.7 μm in size, and predominately in the range of 1 to 2 μm . They were mostly angular in shape, hexagonal and cubic, and some subrounded. In some places, a single belite crystal ($\sim 0.6 \mu\text{m}$) was surrounded by the calcium sulfoaluminate phase, indicating that the enclosing phase was younger. Coarsely crystalline ferrite occurred as an interstitial phase between the crystal grains of belite and calcium sulfoaluminate. Ferrite laths are characteristic for this sample, where well-developed tabular crystals of ferrite, ranging from 0.7 to 2.3 μm in size, are grouped in clusters of cca 20 μm in size (Figure 5a). Mayenite was observed as a dark interstitial phase (Figure 5b), often enclosing calcium sulfoaluminate grains. Particularly for rapid cooling, the equilibrium cooling can hardly be realized, and mayenite would occur in such a case [6]. Periclase occurred as euhedral crystals from 0.6 to 2.7 μm in size. Rarely, needle-like crystals of gehlenite were observed in the matrix, while EDS maps enriched with K indicate arcanite (Figure 4).

The nonlinear cooled clinker also showed a holocrystalline microtexture (Figures 3 and 4). Pores, more or less isometric in shape, were from 5 to 44 μm in size, and elongated pores were also observed. Euhedral to subhedral belite grains were rounded and subangular, 0.7 to 8.5 μm in size, most of them being in the range 2 to 4 μm . Individual grains appeared as irregular. Belite grains were joined together or dispersed in the ferrite phase. Clustered calcium sulfoaluminate crystal grains were generally euhedral, some of them subhedral, cubic and hexagonal in shape (Figure 5c), 0.9 to 4.4 μm in size, and mostly in the range from 1 to 2 μm . Anhedral calcium sulfoaluminate occurred interstitially among belite grains. Individual belite grains enclosed by calcium sulfoaluminate phase were also found. The interstitial phase consisted of coarsely crystalline ferrite, and also in some places as dark anhedral mayenite. Needle-like crystals of gehlenite were quite abundant; coarsely crystalline gehlenite also occurred, for the most part, as the interstitial phase among calcium sulfoaluminate crystals (Figure 5d). Other minor phases, such as periclase (Figure 5e) and arcanite, were also evident from the elemental distribution (Figure 4).

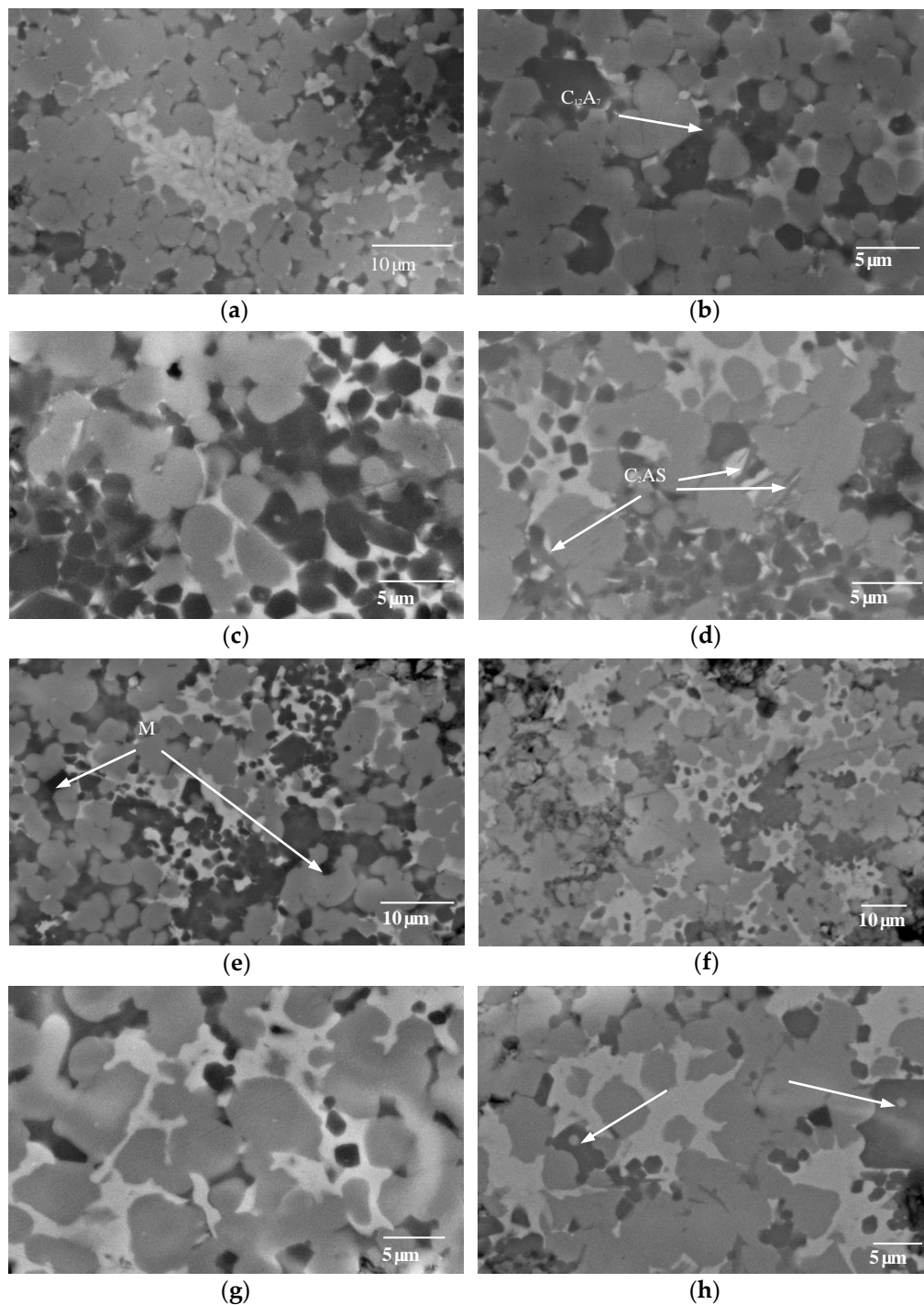


Figure 5. SEM/BSE microphotographs of the investigated clinkers. (a) Clusters of ferrite crystals, air-quenched clinker; (b) mayenite dark interstitial phase, air quenched clinker; (c) six-sided calcium sulfoaluminate crystals, nonlinearly cooled clinker; (d) needle-like gehlenite, linearly cooled clinker; (e) periclase grain, nonlinearly cooled clinker; (f) poikilitic texture, slowly cooled clinker; (g) irregular shaped belite, slowly cooled clinker; (h) calcium sulfoaluminate enclosing belite crystal, slowly cooled clinker.

In the slowly cooled clinker, a holocrystalline and poikilitic texture was evident, with smaller grains of belite and calcium sulfoaluminate completely enclosed in the ferrite phase (Figures 3, 4 and 5f). Pores were rounded to subrounded, mostly isometric, and from 4 to 52 μm in size. Dominant belite grains were from 0.5 to 8.8 μm in size. The majority of grains ranged in size from 4 to 6 μm.

Belite grains were rounded and the majority irregularly-shaped (Figure 5g). Clusters of belite and calcium sulfoaluminate crystal grains were not so evident in this case. In most places, the belite grains were connected to each other by the neck, only rarely were grains dispersed. Calcium sulfoaluminate exhibited euhedral to subhedral crystals, 0.7 to 5.0 μm in size, with most of the grains ranging from 1 to 2 μm in size. Single cubic and six-sided euhedral crystals of calcium sulfoaluminate phase were observed. As shown in Figure 5h, individual belite grains enclosed by the calcium sulfoaluminate phase were also observed in this sample. The preferential distribution of titanium ions in the ferrite phase was also evidenced by partition images obtained by SEM BSE (Figure 4). This cooling led to the gehlenite formation, coarsely crystalline and also needle-like, was more abundant than after the other cooling regimes. Periclase grains, from 1.2 to 3.3 μm in size, occurred in the calcium sulfoaluminate phase, as indicated by the Mg-enriched areas in Figure 4, while the K-enriched spots indicate arcanite.

The microscopical analysis revealed that distribution, morphology, and size of phases varied depending on the different cooling regimes. Moreover, the phase and chemical composition changed with the cooling regime, which could be ascribed to the difference in the crystallization path. Cooling influenced the amount of interstitial phases formed, such as mayenite and gehlenite. Rapid cooling favored the clustering of belite and calcium sulfoaluminate crystal grains. The cooling regime also influenced the form and shape of the phases. While in rapidly cooled samples, mostly euhedral and rounded belite prevailed, subhedral grains (rounded/subrounded) were enhanced under nonlinear cooling and in slow cooling subhedral and anhedral grains with irregular shapes prevailed. In the slowly cooled clinker, calcium sulfoaluminate crystals were better crystallized typically showed sharp edges and a good, euhedral, crystal form. The crystal's appearance in the rapid cooled clinker looked irregular. A higher hydrating rate was observed for clinkers with this kind of calcium sulfoaluminate phase [33].

As seen from Figure 6, the belite grains showed a consistent trend toward larger crystals with slower cooling rates, supporting previous works that faster cooling rates yield smaller silicate crystals [2,34]. In samples subjected to air quenching and nonlinear cooling, the largest amount of grains was observed in the ranges below 4 μm , whereas slow cooling yielded the highest fraction of grains >4 μm . The influence of the cooling regime on the grain size distribution of calcium sulfoaluminate was not as significant, although a slight increase in size was evident with slower cooling rates.

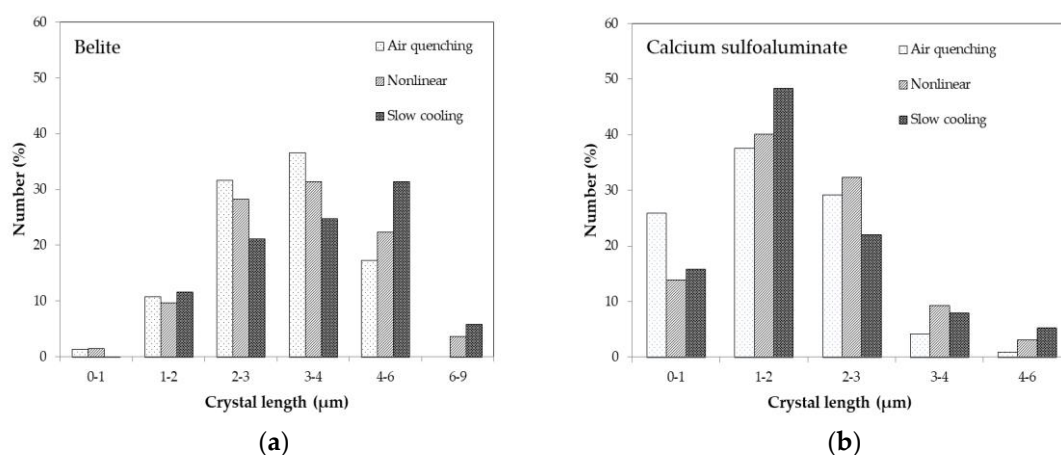


Figure 6. Belite (a) and calcium sulfoaluminate (b) crystal size distributions under different cooling regimes.

Ferrite also appeared differently among the various cooling regimes. In the air quenched clinker, small tabular grains formed. In the nonlinear sample, the ferrite was coarsely crystalline, whereas in the slowly cooled clinker, it exhibited a poikilitic microtexture. The matrix crystals became progressively larger as the cooling rate was reduced. Furthermore, coarsely crystalline gehlenite was characteristic in the slowly cooled clinker, while a needle-like structure prevailed in the clinker, which was nonlinearly cooled.

As indicated by EDS analyses, several substitute elements were incorporated into the main phases (Table 4, Figure 7). Besides being a constituent of ferrite, iron was incorporated in calcium sulfoaluminate, and to a smaller extent also in the belite phase. Titanium, which was introduced into clinkers mainly by bauxite, predominately substituting iron in the ferrite phase, was also identified to a lesser amount in calcium sulfoaluminate, and lastly substituting silicon in belite, as also stated by Kurdowski [35]. To a lesser amount, all three of the main clinker phases also contained alkalis, where potassium and sodium were incorporated primarily in calcium sulfoaluminate, followed by belite and ferrite. On the other hand, magnesium was distributed preferentially in ferrite, then to a lesser extent in calcium sulfoaluminate and belite, while cement clinkers also contained periclase as a separate phase. Ferrite and calcium sulfoaluminate also incorporated large amounts of silicon, while belite contained aluminum, and sulfate was found in ferrite and belite.

Table 4. Average chemical composition (wt.%) of the main phases in the clinkers (determined by EDS analyses).¹

Phase	Cooling	Na	Mg	Al	Si	S	K	Ca	Ti	Fe
Belite	Air quenching	0.27	0.46	3.47	25.88	0.65	0.41	68.25	0.30	1.00
	Nonlinear	0.22	0.46	3.46	23.97	0.51	0.31	69.53	0.31	1.24
	Slow cooling	0.22	0.39	2.80	24.75	0.51	0.29	69.44	0.36	1.24
Calcium sulfoaluminate	Air quenching	0.36	0.79	32.94	7.82	5.39	0.63	48.22	0.38	3.45
	Nonlinear	0.50	0.50	32.78	6.03	5.50	0.70	49.05	0.37	4.56
	Slow cooling	0.35	0.50	35.97	4.85	6.57	0.62	47.07	0.45	3.52
Ferrite	Air quenching	0.21	1.68	15.73	7.26	0.49	0.32	53.12	2.20	19.57
	Nonlinear	0.22	1.13	14.17	7.78	0.99	0.28	52.00	3.58	20.20
	Slow cooling	0.17	1.30	12.26	5.85	0.47	0.20	51.12	4.13	24.50

¹ Total is normalized to be 100 wt.%.

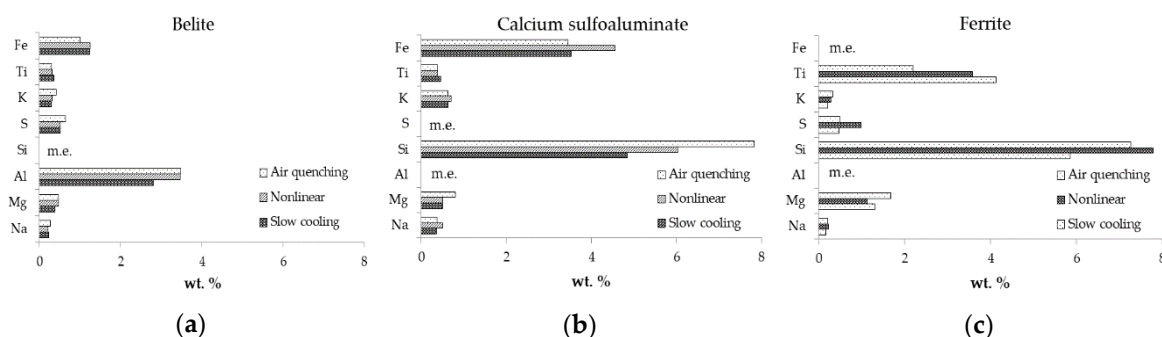


Figure 7. Distribution of substitute elements in the main clinker phases (m.e.: Major element making up the basic lattice of the phase). (a) belite.; (b) Calcium sulfoaluminate; (c) Ferrite.

The chemical composition of the clinker phases varied according to the regime of cooling. Thus, the chief substituent oxide in belite was aluminum, followed by iron. To a lesser extent, magnesium, sulfur, potassium, titanium, and sodium were also incorporated in the phase. The belite in the clinker, which had been slowly cooled, was characterized by a general lack of incorporated foreign ions (5.80% compared to 6.50% and 6.65% for nonlinearly cooled and air quenched clinkers, respectively). This could additionally support the higher content of γ -belite in the slowest cooled clinker, since stabilizing ions in belite prevents the transformation to γ -belite taking place [29]. On the other hand, higher concentrations were observed for the clinkers subject to the other two cooling regimes, indicating that substituent oxides were incorporated to a greater or lesser extent, by substitution at either Ca (Mg, Na, K) or Si sites (Al, Fe, Ti, S). The stabilizing ability of the ions varied significantly, with Al^{3+} cations being quite effective in stabilizing the β -phase [36].

In the calcium sulfoaluminate phase, silicon was identified in the largest concentrations, followed by iron. Titanium, magnesium, potassium, and sodium were also detected in minor amounts. Ye'elimite belongs to the sodalite family of compounds with the general formula $M_4[T_6O_{12}]X$, where T occupies tetrahedral sites and is often Si or Al, M is a low-charge cation (e.g., Na^+ , Ca^{2+} , Sr^{2+}), and X is a charge-balancing anion (e.g., Cl^- , SO_4^{2-} , WO_4^{2-} , CrO_4^{2-} [32]. The highest Si to Al ratio was observed in the air-quenched clinker (0.24 compared to 0.18 and 0.14 for clinkers cooled non-linearly and slowly, respectively), indicating that less Si^{4+} ions are replaced by Al^{3+} ions in relation to the other two clinkers [30,31]. On the other hand, the slowly cooled clinker showed the lowest average Si to Al mass-ratio. Namely, sodalites can have Si/Al ratios ranging from ∞ , for a pure silica framework, to zero, for a pure alumina one such as ye'elimite [37]. Furthermore, the crystalline structure of ye'elimite accepts noticeable amounts of Fe^{3+} instead of Al^{3+} [38,39]. However, the Fe to Al average mass-ratio was lowest in the slowly cooled sample (0.10 compared to 0.11 and 0.14 for the air-quenched and non-linearly cooled clinkers, respectively). The slowly cooled sample also incorporates the highest content of titanium. The highest total amount of minor ions was detected in the air quenched clinker (13.43%), followed by the non-linearly cooled clinker (12.65%), with the smallest amount identified in the slowly cooled clinker (10.3%).

Several substitute ions were incorporated also in the ferrite phase. Among them, silicon was present in the largest amount, followed by titanium, sulfur, magnesium, potassium, and sodium. The lowest total amount of foreign ions in the ferrite was taken up in the slowly cooled clinker (12.12%). Moreover, the Al to Fe average mass-ratio was highest for the air quenched and lowest for the slowly cooled clinker (0.80, 0.70, and 0.50 for the air quenched, nonlinear, and slowly cooled clinkers, respectively). Decreasing Al_2O_3/Fe_2O_3 ratio in the ferrite phase was also reported for Portland cement clinker [9]. The reactivity of ferrite may vary greatly depending on its Al to Fe ratio since it decreases as the iron content increases [40]. Moreover, high iron content increased acidity of the liquid phase [41], which resulted in the dissolution of the belite phase as observed by microscopy. The titanium content in the ferrite phase increased by slow cooling as well. With increasing levels of titanium, the ferrite phase progressively adopts a perovskite-type structure with diminished reactivity [42].

In general, alkalis and magnesium were preferably incorporated by a faster cooling rate. The very high intake of silicon in ferrite and calcium sulfoaluminate was also promoted by the highest cooling rate, which could lead to more gehlenite in the slowly cooled clinker. On the other hand, a larger amount of titanium was identified in the slowly cooled samples, which was especially evident for the ferrite phase. Generally, with an increasing rate of cooling, the concentration of minor ions in the phases increased.

3.3. Isothermal Conduction Calorimetry

The hydraulic reactivity of clinkers cooled following different regimes was investigated by conduction calorimetry (Figure 8).

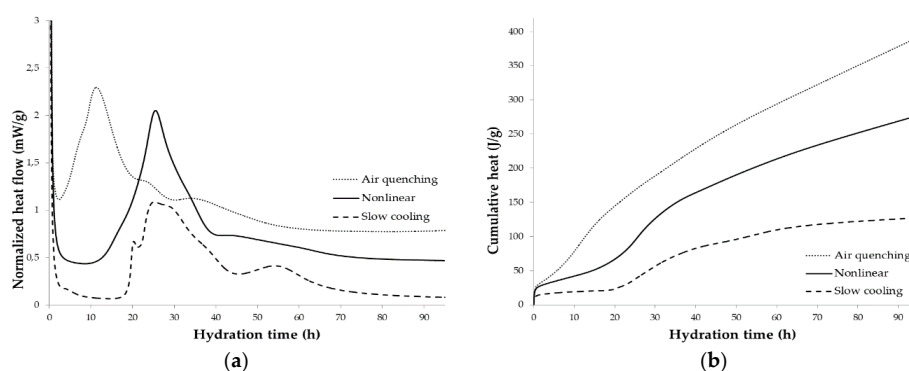


Figure 8. Hydration heat flow (a) and the development of cumulative heat of hydration (b) for the cement clinkers under varying cooling regimes.

Only part of the first exothermic peak was recorded owing to the time required for the premixing procedure outside of the calorimeter and for the calorimeter cell to recover its thermal equilibrium. The first peak occurs immediately when the water is added and can be attributed to the heat of wetting and the very early hydration reactions [43,44]. The variety in reactivity of the clinkers is evident since they exhibit different hydration behaviors. As seen from the results, the air quenched clinker reacted the fastest among the samples (despite having the smallest Blaine specific surface area), which was mainly attributed to the presence of mayenite, which is a highly hydraulic phase, and to the smaller size of the crystals. Namely, hydraulic reactivity is improved with smaller crystals due to the increased surface area [2]. The induction period following event 1 is very short in this sample, only lasting about 30 min. The main peak at 10 h was followed by shoulders at 22 h and 34 h. This heat event covers the main part of the hydration reactions and is responsible for the setting and hardening of the paste [43]. After about 40 h, the rate of hydration slows; most of the heat evolution occurs between 10 h and 40 h, as indicated by the total heat evolution curve. The main peak of the nonlinear cooling occurred at around 25 h, however, a shoulder was observed at around 44 h. The calorimetric curve of the clinker samples being cooled at a constant rate of 1 °C/min showed more peaks, suggesting a more complex hydration evolution. After the first exothermic peak, a small peak followed, and then there was a long induction period, lasting 16 h. This was followed by a peak at 24 h, with two shoulders at 18 h and 36 h, and then a broader peak at 55 h. This sample contained higher amounts of feebly hydraulic gehlenite and non-hydraulic γ -belite. Slow cooling also decreased the hydraulic reactivity of phases due to a reduced concentration of minor ions, as indicated in the main phases. By entering into solid solution in the clinker phases, the transitional metals have the potential to create defect or otherwise stress the crystal lattice and increase hydraulic activity [42]. Furthermore, the reactivity of ferrite was lower in this sample, as indicated by its low Al/Fe ratio, which could also alter the hydraulic reactivity of the clinker.

After 4 days, the cumulative heat from hydration was smallest in the clinker exposed to the slowest rate of cooling (127.3 J/g), and highest in the clinker that had been air quenched (393.1 J/g; Figure 8b). This is probably due to the lower degree of hydration during slow cooling and the highest degree of hydration through air quenching. It can also be observed that the slope of the cumulative curve is sharpest for the air quenched clinker and the least steep for the clinker exposed to slow cooling, indicating that the reaction is fastest in the air quenched clinker and slowest in the clinker exposed to slow cooling.

With regard to the cements prepared from the studied clinkers, the sample of the air quenched clinkers reacted the fastest and released the most heat, while the two cements prepared from the other clinkers reacted comparably (Figure 9). Cements prepared from the slow and nonlinearly cooled clinkers yield similar hydration behavior, showing a longer induction period of hydration (until about 6 h), followed by the main hydration peak with a maximum at 7 h, related to the formation of ettringite [45]. Nevertheless, the total heat from hydration after 4 days was smallest for the cement prepared with clinker with the slowest rate of cooling (149.0 J/g), indicating a lower degree of hydration, and highest for the cement prepared with the air quenched clinker (177.6 J/g).

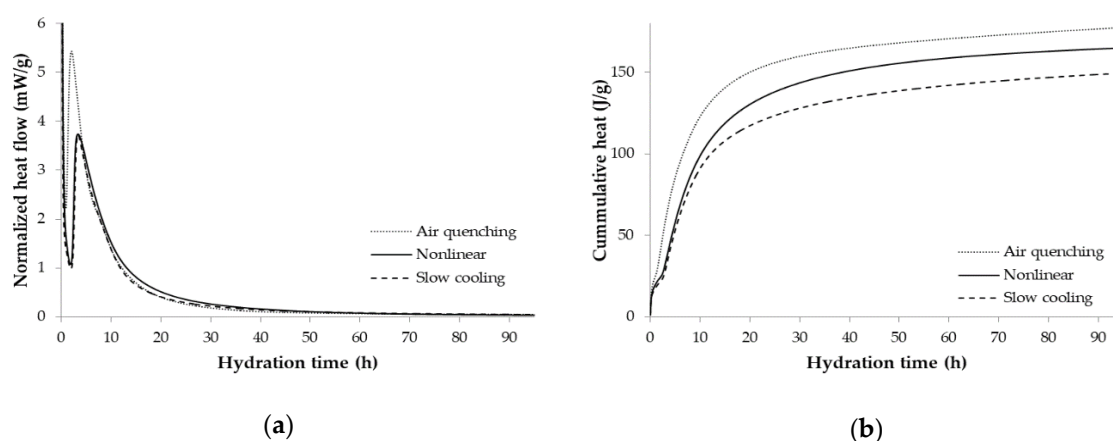


Figure 9. Hydration heat flow (a) and the development of cumulative heat of hydration (b) for the cements under varying cooling regimes.

3.4. Compressive Strength

As seen from the results in Table 5, the compressive strength of cement after 7 days of curing varied slightly according to the cooling regime under which the clinkers had been synthesized. The highest compressive strength was observed in the cements made from the air quenched clinker, relatively closely followed by the non-linearly cooled sample. The compressive strength of the sample, which had been subjected to slow linear cooling, was significantly lower.

Table 5. Compressive strength (at 7 days) of cement made from clinkers exposed to varying cooling regimes.

Compressive Strength	Air Quenching	Nonlinear	Slow Cooling
N/mm ²	18.8 ± 0.7	17.9 ± 1.2	11.5 ± 0.2

In general, the compressive strength of the studied clinkers decreased as the cooling rate slowed. Kohl [34] compared OPC clinker cooling rates to physical cement strength tests, where rapid to moderate cooling increased the 28-day strength. Additionally, Bullard (2015) [2] also showed that very slow cooling of OPC clinkers decreased strength at all ages. It is interesting to note that the sample made from the slowly cooled clinker developed low compressive strength, despite having the highest Blaine fineness, which could be attributed to its phase composition and microstructure. In addition to larger crystal grains, the lower compressive strength of the slowly cooled clinker sample could, therefore, be attributed to the presence of phases with poor hydraulic properties, such as gehlenite [27,46]. On the contrary, mayenite is a highly hydraulic phase and contributed to the higher compressive strength of cement produced from clinkers, which had been air quenched or non-linearly cooled in this study.

4. Conclusions

This contribution presents results on the influence of different cooling regimes on the mineralogy and reactivity of cement clinkers based on belite-sulfoaluminate.

Results showed that the type of cooling regime influenced the phase assemblage of clinkers as well as the morphology and size of the main clinker phases. In addition to the three targeted main phases (belite, calcium sulfoaluminate, and ferrite), clinkers also contained periclase, perovskite, and arcanite, as well as gehlenite and mayenite as minor phases. The ratios of mayenite and gehlenite depended predominately on the cooling rate. Whereas the highly hydraulic mayenite was promoted by rapid cooling, the feebly hydraulic phase gehlenite was formed during slow cooling. The overall

sizes of belite grains were largest in the clinker subjected to slow linear cooling, but such an influence was less evident in the case of calcium sulfoaluminate. Ferrite occurred as an interstitial phase, which, together with small rounded belite and angular calcium sulfoaluminate grains, formed a poikilitic microtexture, especially in the sample subjected to slow linear cooling.

The microstructure influenced the clinkers' reactivity, since the air cooled clinker, which consisted of phase grains with smaller sizes overall, reacted more rapidly than those clinkers, which had been cooled at slower rates. Moreover, air quenching increases the chances of other elements being incorporated into the clinker phases, resulting in the formation of more reactive ferrite and calcium sulfoaluminate, and stabilizing β -belite. The compressive strength of cement decreased with lower cooling rates, with the air quenched clinker exhibiting the highest value of compressive strength at 7 days.

The overall results of the study indicated that within the belite-calcium sulfoaluminate-ferrite system, among the three cooling regimes studied, air quenching resulted in the most reactive cement clinker and in a higher compressive strength of cement. Highly reactive mayenite was formed with rapid cooling of the clinker, whilst the formation of non-hydraulic (γ -belite) or poorly hydraulic (gehlenite) phases, were respectively diminished or prevented.

Author Contributions: Conceptualization, S.D. and L.Ž.; methodology, S.D., A.I. and L.Ž.; analysis, K.Š., L.Ž., S.D., K.N., M.B.; writing—original draft preparation, S.D.; writing—review and editing, S.D., L.Ž., A.I., K.Š.; funding acquisition, S.D., L.Ž., A.I. All authors have read and agreed to the published version of the manuscript.

Funding: Project No. C3330-17-529035 "Raziskovalci-2.0-ZAG-529035" was granted by the Ministry of Education, Science and Sport of the Republic of Slovenia. The investment is co-financed by the Republic of Slovenia, Ministry of Education, Science and Sport and the European Regional Development Fund.

Acknowledgments: The Metrology Institute of the Republic of Slovenia is acknowledged for the use of XRF.

Conflicts of Interest: The authors declare no conflict of interest.

References

1. Ono, Y. Microscopical Observations of Clinker for the Estimation of Burning Condition. Grindability, and Hydraulic Activity. In Proceedings of the Third International Conference on Cement Microscopy, International Cement Microscopy Association, Houston, TX, USA, 19–21 March 1981; pp. 198–210.
2. Bullard, R.A. Effect of Cooling Rates on Mineralization in Portland Cement Clinker. Ph.D. Thesis, University of Missouri-Columbia, Columbia, MO, USA, 2015.
3. Telschow, S.; Dam-Johansen, K.; Jappe Frandsen, F.; Wedel, S.; Theisen, K. Clinker Burning Kinetics and Mechanism. Ph.D. Thesis, Technical University of Denmark, Lyngby, Denmark, 2012.
4. Staněk, T.; Sulovský, P. The Impact of Basic Minor Oxides on the Clinker Formation. *Mater. Sci. Forum* **2017**, *908*, 3–9. [[CrossRef](#)]
5. Ward, G.W. Effect of heat treatment and cooling rate on the microscopic structure of portland cement clinker. *J. Res. Natl. Bur. Stan.* **1941**, *26*, 49. [[CrossRef](#)]
6. Hong, H.; Fu, Z.; Min, X. Effect of cooling performance on the mineralogical character of Portland cement clinker. *Cem. Concr. Res.* **2001**, *31*, 287–290. [[CrossRef](#)]
7. Sazonova, N.A.; Skripnikova, N.K. Using the low-temperature plasma in cement production. *J. Phys. Conf. Ser.* **2015**, *652*, 012063. [[CrossRef](#)]
8. Maki, I. Processing Conditions of Portland Cement Clinker as Viewed from the Fine Textures of the Constituent Minerals. *Ceram. Trans.* **1994**, *40*, 3–17.
9. Ichikawa, M.; Ikeda, S.; Komukai, Y. Effect of cooling rate and Na₂O content on the character of the interstitial materials in portland cement clinker. *Cem. Concr. Res.* **1994**, *24*, 5.
10. Fukuda, K.; Maki, I.; Ikeda, S.; Ito, S. Microtextures Formed by the Remelting Reaction in Belite Crystals. *J. Am. Ceram. Soc.* **1993**, *76*, 2942–2944. [[CrossRef](#)]
11. Martín-Sedeño, M.C.; Cuberos, A.J.M.; De la Torre, Á.G.; Álvarez-Pinazo, G.; Ordóñez, L.M.; Gateshki, M.; Aranda, M.A.G. Aluminum-rich belite sulfoaluminate cements: Clinkering and early age hydration. *Cem. Concr. Res.* **2010**, *40*, 359–369. [[CrossRef](#)]

12. Ma, B.; Li, X.; Shen, X.; Mao, Y.; Huang, H. Enhancing the addition of fly ash from thermal power plants in activated high belite sulfoaluminate cement. *Constr. Build. Mater.* **2014**, *52*, 261–266. [[CrossRef](#)]
13. Bullerjahn, F.; Schmitt, D.; Ben Haha, M. Effect of raw mix design and of clinkering process on the formation and mineralogical composition of (ternesite) belite calcium sulfoaluminate ferrite clinker. *Cem. Concr. Res.* **2014**, *59*, 87–95. [[CrossRef](#)]
14. De la Torre, Á.G.; Cuberos, A.J.M.; Álvarez-Pinazo, G.; Cuesta, A.; Aranda, M.A.G. In situ powder diffraction study of belite sulfoaluminate clinkering. *J. Synchrotron Rad.* **2011**, *18*, 506–514. [[CrossRef](#)]
15. Ma, S.; Snellings, R.; Li, X.; Shen, X.; Scrivener, K.L. Alite-ye’elimate cement: Synthesis and mineralogical analysis. *Cem. Concr. Res.* **2013**, *45*, 15–20. [[CrossRef](#)]
16. Quillin, K. Performance of belite–sulfoaluminate cements. *Cem. Concr. Res.* **2001**, *31*, 1341–1349. [[CrossRef](#)]
17. Gartner, E.; Sui, T. Alternative cement clinkers. *Cem. Concr. Res.* **2018**, *114*, 27–39. [[CrossRef](#)]
18. Liu, G.Q.; Yang, Q.X.; Jiang, L.; Xue, P.; Zhang, X.L.; Han, F.L. Sintering characteristics of BCSAF cement clinker with added wastes from production of manganese and magnesium metals. *Adv. Cem. Res.* **2017**, 1–9. [[CrossRef](#)]
19. Cuberos, A.J.M.; De la Torre, Á.G.; Álvarez-Pinazo, G.; Martín-Sedeño, M.C.; Schollbach, K.; Pöllmann, H.; Aranda, M.A.G. Active Iron-Rich Belite Sulfoaluminate Cements: Clinkering and Hydration. *Environ. Sci. Technol.* **2010**, *44*, 6855–6862. [[CrossRef](#)] [[PubMed](#)]
20. Aranda, M.A.G.; Cuberos, A.J.M.; Cuesta, A.; Alvarez-Pinazo, G.; De la Torre, A.G.; Schollbach, K.; Pollmann, H. Hydrating behaviour of activated belite sulfoaluminate cements. In Proceedings of the 13th International Congress on the Chemistry of Cement, Madrid, Spain, 3–8 July 2011.
21. Senff, L.; Castela, A.; Hajjaji, W.; Hotza, D.; Labrincha, J.A. Formulations of sulfobelite cement through design of experiments. *Constr. Build. Mater.* **2011**, *25*, 3410–3416. [[CrossRef](#)]
22. Da Costa, E.B.; Rodríguez, E.D.; Bernal, S.A.; Provis, J.L.; Gobbo, L.A.; Kirchheim, A.P. Production and hydration of calcium sulfoaluminate-belite cements derived from aluminium anodising sludge. *Constr. Build. Mater.* **2016**, *122*, 373–383. [[CrossRef](#)]
23. Dieneman, W.; Schmitt, D.; Bullerjahn, F.; Ben Haha, M. Belite-Calciumsulfoaluminate-Ternesite (BCT)-A new low-carbon clinker Technology. *Cem. Int.* **2013**, *11*, 100–109.
24. Arjunan, P.; Silsbee, M.R.; Della, M. Roy Sulfoaluminate-belite cement from low-calcium fly ash and sulfur-rich and other industrial by-products. *Cem. Concr. Res.* **1999**, *29*, 1305–1311. [[CrossRef](#)]
25. Chen, I.A.; Juenger, M.C.G. Synthesis and hydration of calcium sulfoaluminate-belite cements with varied phase compositions. *J. Mater. Sci.* **2011**, *46*, 2568–2577. [[CrossRef](#)]
26. Álvarez-Pinazo, G.; Cuesta, A.; García-Maté, M.; Santacruz, I.; Losilla, E.R.; la Torre, A.G.D.; León-Reina, L.; Aranda, M.A.G. Rietveld quantitative phase analysis of Yeelimate-containing cements. *Cem. Concr. Res.* **2012**, *42*, 960–971. [[CrossRef](#)]
27. Wang, W.; Wang, X.; Zhu, J.; Wang, P.; Ma, C. Experimental Investigation and Modeling of Sulfoaluminate Cement Preparation Using Desulfurization Gypsum and Red Mud. *Ind. Eng. Chem. Res.* **2013**, *52*, 1261–1266. [[CrossRef](#)]
28. Borštnar, M.; Daneu, N.; Dolenc, S. Phase development and hydration kinetics of belite-calcium sulfoaluminate cements at different curing temperatures. *Ceram. Int.* **2020**. [[CrossRef](#)]
29. Taylor, H.F.W. *Cement Chemistry*, 2nd ed.; T. Telford: London, UK, 1997; ISBN 978-0-7277-2592-9.
30. Cuesta, A.; De la Torre, A.G.; Losilla, E.R.; Peterson, V.K.; Rejmak, P.; Ayuela, A.; Frontera, C.; Aranda, M.A.G. Structure, Atomistic Simulations, and Phase Transition of Stoichiometric Yeelimate. *Chem. Mater.* **2013**, *25*, 1680–1687. [[CrossRef](#)]
31. Hargis, C.W.; Moon, J.; Lothenbach, B.; Winnefeld, F.; Wenk, H.-R.; Monteiro, P.J.M. Calcium Sulfoaluminate Sodalite (Ca₄Al₆O₁₂SO₄) Crystal Structure Evaluation and Bulk Modulus Determination. *J. Am. Ceram. Soc.* **2014**, *97*, 892–898. [[CrossRef](#)]
32. Pedersen, M.T.; Jensen, F.; Skibsted, J. Structural Investigation of Ye’elimate, Ca₄Al₆O₁₂SO₄, by ²⁷Al MAS and MQMAS NMR at Different Magnetic Fields. *J. Phys. Chem. C* **2018**, *122*, 12077–12089. [[CrossRef](#)]
33. Muzhen, S.; Junan d Zongdao, W.; Xiaoxin, L. Research on the chemical composition and microstructures of sulho-aluminate cement clinker.
34. Kohl, R.F. *Effects of Cooling Rate*; Portland Cement Association: Skokie, IL, USA, 1979; Kiln Paper No. 24; pp. 1–23.
35. Kurdowski, W. *Cement and Concrete Chemistry*; Springer: Cham, The Netherlands, 2014; ISBN 978-94-007-7944-0.

36. Cuesta, A.; Aranda, M.A.G.; Sanz, J.; de la Torre, Á.G.; Losilla, E.R. Mechanism of stabilization of dicalcium silicate solid solution with aluminium. *Dalton Trans.* **2014**, *43*, 2176–2182. [[CrossRef](#)]
37. Moteki, T.; Chaikittisilp, W.; Shimojima, A.; Okubo, T. Silica Sodalite without Occluded Organic Matters by Topotactic Conversion of Lamellar Precursor. *J. Am. Chem. Soc.* **2008**, *130*, 15780. [[CrossRef](#)]
38. Fortes, G.M.; Lourenço, R.R.; Montini, M.; Gallo, J.B.; Rodrigues, J.D.A. Synthesis and Mechanical Characterization of Iron Oxide Rich Sulfolite Cements Prepared Using Bauxite Residue. *Mat. Res.* **2016**, *19*, 276–284. [[CrossRef](#)]
39. Idrissi, M.; Diouri, A.; Damidot, D.; Greneche, J.M.; Talbi, M.A.; Taibi, M. Characterisation of iron inclusion during the formation of calcium sulfoaluminate phase. *Cem. Concr. Res.* **2010**, *40*, 1314–1319. [[CrossRef](#)]
40. Gartner, E.M.; Young, J.F.; Damidot, D.A.; Jawed, I. Hydration of Portland cement. In *Structure and Performance of Cements*, 2nd ed.; Bensted, J., Barnes, P., Eds.; Spon Press: London, UK, 2002; pp. 83–84.
41. Odigure, J.O. Kinetic modelling of cement raw mix containing iron particles and clinker microstructure. *Cem. Concr. Res.* **1996**, *26*, 1435–1442. [[CrossRef](#)]
42. Moir, G.K.; Glasser, F.P. Mineralisers, modifiers and activators in the clinkering process, Mineralisers, modifiers and activators in the clinkering process. In Proceedings of the 9th International Congress on the Chemistry of Cement, Delhi, India, 23–28 November 1992; Volume 1, pp. 125–152.
43. Winnefeld, F.; Barlag, S. Calorimetric and thermogravimetric study on the influence of calcium sulfate on the hydration of ye’elimite. *J. Therm. Anal. Calorim.* **2010**, *101*, 949–957. [[CrossRef](#)]
44. Shen, Y.; Chen, X.; Zhang, W.; Li, X. Effect of ternesite on the hydration and properties of calcium sulfoaluminate cement. *J. Therm. Anal. Calorim.* **2019**, *136*, 687–695. [[CrossRef](#)]
45. Winnefeld, F.; Martin, L.H.J.; Müller, C.J.; Lothenbach, B. Using gypsum to control hydration kinetics of CSA cements. *Constr. Build. Mater.* **2017**, *155*, 154–163. [[CrossRef](#)]
46. West, A.R. *Solid State Chemistry and Its Applications*; John Wiley and Sons, Inc.: Hoboken, NJ, USA, 2014; p. 584.

Publisher’s Note: MDPI stays neutral with regard to jurisdictional claims in published maps and institutional affiliations.



© 2020 by the authors. Licensee MDPI, Basel, Switzerland. This article is an open access article distributed under the terms and conditions of the Creative Commons Attribution (CC BY) license (<http://creativecommons.org/licenses/by/4.0/>).